Geophysical Journal International

Geophys. J. Int. (2015) **202,** 1021–1028
GJI Geodynamics and tectonics

doi: 10.1093/gji/ggv207

A comparison of strain rates and seismicity for Fennoscandia: depth dependency of deformation from glacial isostatic adjustment

M. Keiding,[1] C. Kreemer,[2] C.D. Lindholm,[3] S. Gradmann,[1] O. Olesen[1] and H.P. Kierulf[4]

[1] *Geological Survey of Norway, Trondheim, Norway. E-mail: marie.keiding@ngu.no*
[2] *Nevada Bureau of Mines and Geology, and Seismological Laboratory, University of Nevada, Reno, NV 89557, USA*
[3] *NORSAR, Kjeller, Norway*
[4] *Geodetic Institute, Norwegian Mapping Authority, Hønefoss, Norway*

Accepted 2015 May 14. Received 2015 May 13; in original form 2015 February 24

SUMMARY

We investigate the influence of the glacial isostatic adjustment (GIA) on the deformation at the surface and at seismogenic depths in Fennoscandia. The surface strain rate field, derived from geodetic data, is controlled by GIA which causes NW–SE extension of up to 4×10^{-9} yr^{-1} in most of mainland Fennoscandia, surrounded by regions of radial shortening towards the centre of uplift. The seismic deformation field, derived from a new compilation of focal mechanisms, shows consistent NW–SE compression on the Norwegian continental margin and a tendency towards tension in mainland Fennoscandia. The seismic moment rate is at least two orders of magnitude smaller than the geodetic moment rate. We propose that the low level of seismicity and the tendency towards tensional focal mechanisms in mainland Fennoscandia may be explained by the destructive interference of the regional stress from ridge push with the flexural stress due to GIA.

Key words: Seismicity and tectonics; Intra-plate processes; Lithospheric flexure; Neotectonics.

1 INTRODUCTION

It is generally accepted that the interseismic surface strain rates in plate boundary zones reflect crustal strain rates (e.g. Kreemer *et al.* 2014), which are related to seismicity through the seismic coupling (Bird & Kagan 2004). However, the relationship between strain rates at the surface and deformation at seismogenic depths is not well known in intraplate regions undergoing glacial isostatic adjustment (GIA), and the influence of GIA on present-day seismicity is still debated.

At the peak of the last glaciation around 20 000 yr ago, most of Canada and northern United States (the Laurentide region), Scotland and Fennoscandia were covered under up to 2–3 km thick ice sheets. Within the latest phase of the deglaciation, around 10 000 yr ago, an extraordinary pulse of seismicity occurred in northern Fennoscandia, likely due to a combination of crustal deweighting, high pore pressures and long-term tectonic compression (Muir Wood 1989b; Lund *et al.* 2009). The seismicity probably included a number of $M > 7$ earthquakes and resulted in prominent, up to 155 km long fault scarps as well as coincident land slides and liquefaction phenomena (e.g. Lagerbäck 1992; Dehls *et al.* 2000; Olesen *et al.* 2013a).

Today, seismicity remains relatively high in both Fennoscandia and the Laurentide region. Several authors have argued that the GIA is at least partially responsible for the elevated seismicity in parts of the Laurentide region (e.g. Stein *et al.* 1979; Wu & Johnston 2000; Mazzotti *et al.* 2005) and Fennoscandia (Arvidsson 1996; Hicks *et al.* 2000b; Muir-Wood 2000). For example, Hasegawa & Basham (1989) noted the correlation of high levels of seismicity, steep gradients in free-air gravity and steep gradient in postglacial uplift along the northeastern periphery of the Canadian shield and concluded that there may be a causal relationship.

With this work, we investigate the deformation at the surface and at seismogenic depths in Fennoscandia, and discuss the implications for the question how GIA affects the seismicity.

2 PRESENT-DAY DEFORMATION IN FENNOSCANDIA

Here, we present an overview of the present-day deformation in Fennoscandia and the data that are included in the following analyses.

2.1 Surface deformation

The first-order pattern of surface deformation in Fennoscandia is dominated by GIA, which has been constrained by a number of

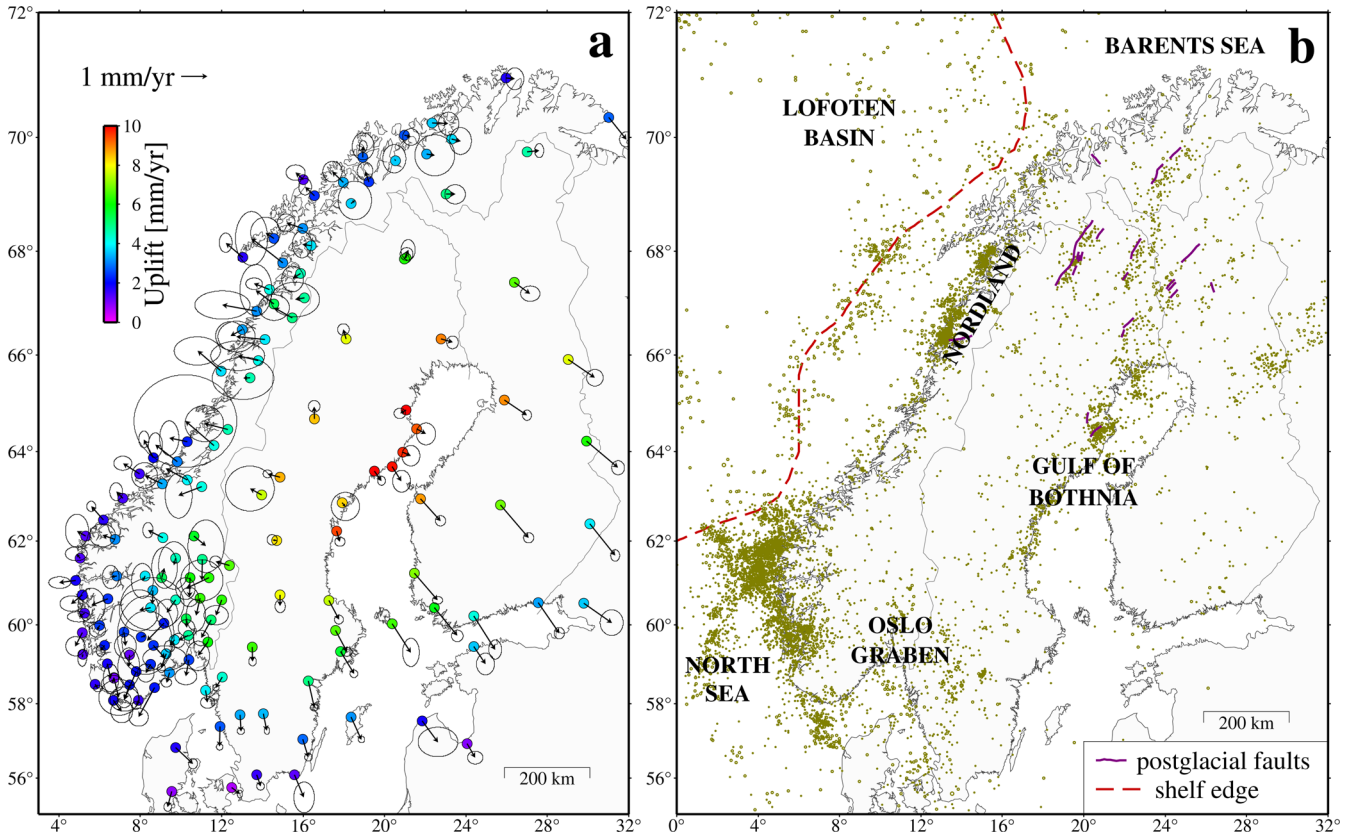

Figure 1. (a) GPS velocities from Kierulf *et al.* (2014) with 95 per cent confidence ellipses. The ITRF2008 velocities are referenced to the stable Eurasian frame. (b) Earthquakes during 1980–2011 from the FENCAT catalogue.

independent data sets, notably tide gauges, gravity change, levelling and GPS data (for a review, see Steffen & Wu 2011). A joint effort to study the GIA by means of GPS data was launched in the early 1990s with the BIFROST project (e.g. Lidberg *et al.* 2010) through which a GPS network with a typical spacing of 100–200 km between neighbouring stations was established in Fennoscandia. GPS data from the BIFROST network have been combined with results from levelling and tide-gauge measurements to get detailed constraints on the uplift in Fennoscandia (Vestøl 2006). The GPS velocity field of Norway was analysed by Kierulf *et al.* (2013), who included stations mainly established for navigational purposes in addition to the stations built for crustal deformation studies. Finally, Kierulf *et al.* (2014) combined data from the spatially dense Norwegian network with data from the BIFROST network and other high-quality GPS stations in north-central Europe to produce a new GPS velocity field for Fennoscandia (see Fig. 1a). The GIA causes uplift of up to 10 mm yr^{-1} in the northern part of the Gulf of Bothnia, decreasing to 1–2 mm yr^{-1} along the southern coast of Norway. The horizontal velocity field is also to a first order controlled by the uplift, which causes outward spreading of 1–2 mm yr^{-1} relative to the uplift centre (Kierulf *et al.* 2014).

2.2 Seismicity

A catalogue of the seismicity in Fennoscandia dating back to year 1375 is available from the joint Nordic earthquake bulletin, FENCAT, maintained by University of Helsinki (e.g. Mäntyniemi *et al.* 2004). Fig. 1(b) shows all earthquakes from FENCAT during 1980–2011. The seismicity in Fennoscandia is low to intermediate in intensity and mainly located in the upper 20 km of the crust. The highest seismicity occurs in the rifted continental margin, particularly along the shelf-edge and in the strongly faulted regions near the failed rifts in the North Sea and near the coast of southwestern Norway (e.g. Lindholm *et al.* 2005). The oceanic crust is mostly aseismic, however, unusually high seismic activity occurs in the eastern Lofoten Basin, possibly due to local flexure of the lithosphere related to rapid deposition of glacial sediments (Byrkjeland *et al.* 2000).

In mainland Fennoscandia, the seismicity is mostly low, both in terms of frequency and magnitude, but there are a few exceptions to this. A major occurrence of seismicity is southwestern Norway, a region strongly faulted by post-Caledonian faults and shear zones (Bøe *et al.* 2010). Another important occurrence of seismicity is Nordland (see Fig. 1b), where two shallow earthquake swarms occurred in recent years (Bungum *et al.* 1982; Atakan *et al.* 1994). The largest known historical earthquake in Fennoscandia occurred in Nordland in 1819 and has been estimated to have a $M_S = 5.8$ (Muir Wood 1989a; Bungum & Olesen 2005). At present-day, the seismicity in Nordland is characterized by swarm activity with magnitudes rarely reaching 4. Microseismicity is associated with the postglacial faults in northern Fennoscandia (Arvidsson 1996; Lindblom *et al.* 2015). Some seismicity also occurs along the Swedish coast in the Gulf of Bothnia and in southern Sweden and the Oslo Graben.

2.3 Focal mechanisms

The most recent compilation of earthquake focal mechanisms in Norway included 112 mechanisms and was presented by Hicks *et al.* (2000a). Here, we present a new compilation of focal mechanisms in Norway including an additional three published

Table 1. Previously unpublished earthquake focal mechanisms in Norway.

Date	Latitude	Longitude	Depth	ML	T-tr	T-pl	P-tr	P-pl	Strike	Dip	Rake	Quality
2000.11.26	60.038	5.474	11	2.6	307	52	66	21	116	36	31	B
2000.11.29	59.851	6.980	15	2.6	205	3	115	8	250	82	−176	B
2000.12.08	60.131	4.786	4	3.8	174	8	73	53	230	48	−141	A
2001.06.22	60.105	7.352	15	2.6	175	4	265	9	310	81	−4	B
2003.12.15	61.674	2.653	10	3.3	200	6	292	24	334	69	−13	B
2010.12.20	59.900	5.366	17	3.3	14	10	279	28	60	63	−167	B
2012.03.24	60.634	6.401	15.3	3.0	16	17	281	14	58	68	178	A

T, tensional axis; P, compressional axis; tr, trend; pl, plunge.

mechanisms (Hicks & Ottemöller 2001; Ottemöller *et al.* 2005; Sørensen *et al.* 2007), seven previously unpublished mechanisms from the Norwegian National Seismic Network (Table 1) and seven mechanisms from the Global CMT Project (Ekström *et al.* 2012). This new compilation of Norwegian focal mechanisms is, to the best of our knowledge, complete. In the following analysis, we also include 109 published mechanisms for Sweden, Finland and Baltica (Slunga 1979; Slunga & Ahjos 1986; Henderson 1991; Arvidsson & Kulhanek 1994; Uski *et al.* 2003, 2006; Juhlin & Lund 2011; Smedberg *et al.* 2012). The compilation of Fennoscandian focal mechanisms is presented in Table S1 and Fig. S1 in the supplementary material.

The focal mechanisms on the continental margin are relatively deep, with depths below 9 km, and are typically reverse to strike-slip with WNW–ESE to NW–SE trending axes of compression, aligning approximately with the spreading direction from the mid-Atlantic ridge (Hicks *et al.* 2000a). The mechanisms in mainland Fennoscandia are often shallower than on the continental margin and show larger variation in style and direction. Mechanisms around the postglacial faults in northern Fennoscandia are mostly reverse, but normal faulting and strike-slip are common elsewhere. A small number of Swedish mechanisms seem to be located in the deeper parts of the lower crust, with focal depths as deep as 40 km (Arvidsson & Kulhanek 1994).

3 SURFACE STRAIN RATE FIELD

We estimate strain rates from the horizontal velocities of Kierulf *et al.* (2014), using the method of Haines and Holt (for a detailed review of the methodology, see Holt *et al.* 2000; Beavan & Haines 2001). The method assumes that the lithosphere behaves as a continuum. The observed velocity field is parameterized using a rotation vector function at the surface of a sphere, and the rotation vector function is then expanded on a curvilinear grid using bi-cubic Bessel interpolation. The distribution of GPS stations in the velocity field of Kierulf *et al.* (2014) is irregular, as the GPS network in Norway includes a large number of stations that were installed for navigational purposes. Thus, it is difficult to define a grid that fits the station distribution perfectly everywhere. As the GPS network in Norway includes many stations with larger uncertainties, we choose to use a rather coarse grid, with cell size of approximately 2° longitude by 1° latitude, which allows for some smoothing in Norway and fits well the station distribution in rest of Fennoscandia. The strain rate method requires as input an *a priori* strain rate variance for each grid cell, and this *a priori* variance controls the balance between the fit to the data and the smoothness of the interpolated velocity field. The surface deformation in Fennoscandia is characterized by diffuse, intraplate deformation everywhere, thus we apply a uniform *a priori* strain rate variance for all grid cells, and we choose a value which results in a fit to the observed velocities with a reduced chi-squared of 2.0. Finally, the strain rates are calculated as the spatial derivatives of the interpolated velocity field:

$$\dot{\epsilon}_{xx} = \frac{\partial v_x}{\partial x}, \quad \dot{\epsilon}_{yy} = \frac{\partial v_y}{\partial y}, \quad \dot{\epsilon}_{xy} = \frac{1}{2}\left(\frac{\partial v_x}{\partial y} + \frac{\partial v_y}{\partial x}\right), \tag{1}$$

where v is velocity, x is longitude and y is latitude.

The results are presented in Fig. 2(a) as the principal strain rates as well as the areal strain rate, defined as $\frac{1}{2}(\dot{\epsilon}_{xx} + \dot{\epsilon}_{yy})$. An NE–SW elongated signal of expansion covers most of Fennoscandia, closely resembling the pattern of the glacial isostatic uplift bulge. The highest areal strain rates are seen in the Gulf of Bothnia and south-central Sweden. The region of expansion is surrounded by regions of contraction. The transition from expansion to contraction follows the Finnish border to Russia, crosses southern Sweden and southern Norway and runs along the western coast of Norway up to the Barents Sea. Along the western coast of Norway, several of the outermost GPS stations lie in the region of contraction, indicating that the areal expansion does not extend into the offshore regions. This is, however, not the case along the northern coast of Norway, where the signal of expansion extends to the outermost GPS stations, indicating that the change from expansion to contraction occurs offshore. The notion that parts of the Barents Sea are currently undergoing expansion is consistent with flexural uplift, as observed by 800–1000 m erosion in the southern Barents Sea during the Plio-Pleistocene (Riis & Fjeldskaar 1992).

The principal strain rates are plotted on top of the areal strain rates in Fig. 2(a). Within the region of expansion, they show a consistent pattern of up to 4×10^{-9} yr^{-1} extension in the NW–SE direction. The dominant NW–SE direction of extension is caused by the NE–SW elongation of the uplift bulge in Fennoscandia. The only marked deviation from this pattern is seen in southwestern Norway, where the extension is rotated towards N–S, consistent with the continuation of the uplift bulge towards Scotland. In the regions of contraction that surround the broad signal of areal expansion, the principal shortening axis always trends radially away from the centre of uplift. An earlier study of the strain rates in northern Europe showed a similar radial pattern of shortening in north-central Europe (Nocquet *et al.* 2005).

We obtain a minimum estimate of the geodetic moment rate, using the formula (Holt *et al.* 1995)

$$\dot{M}_0^G = 2\mu V \left(\left| \frac{1}{2}(\dot{\epsilon}_{xx} + \dot{\epsilon}_{yy}) \right| + \sqrt{\frac{1}{4}(\dot{\epsilon}_{xx} - \dot{\epsilon}_{yy})^2 + \dot{\epsilon}_{xy}{}^2} \right), \tag{2}$$

where μ is the shear modulus (here we use $\mu = 32$ GPa) and V is the cell volume calculated as the grid cell area multiplied by the seismogenic thickness (here we use 20 km based on the typical depth of seismicity in the region). The geodetic moment rate gives an estimate of how much moment is accumulating, assuming that the strain rates at the surface are representative of the strain rate in the seismogenic part of the crust. The formula assumes that the

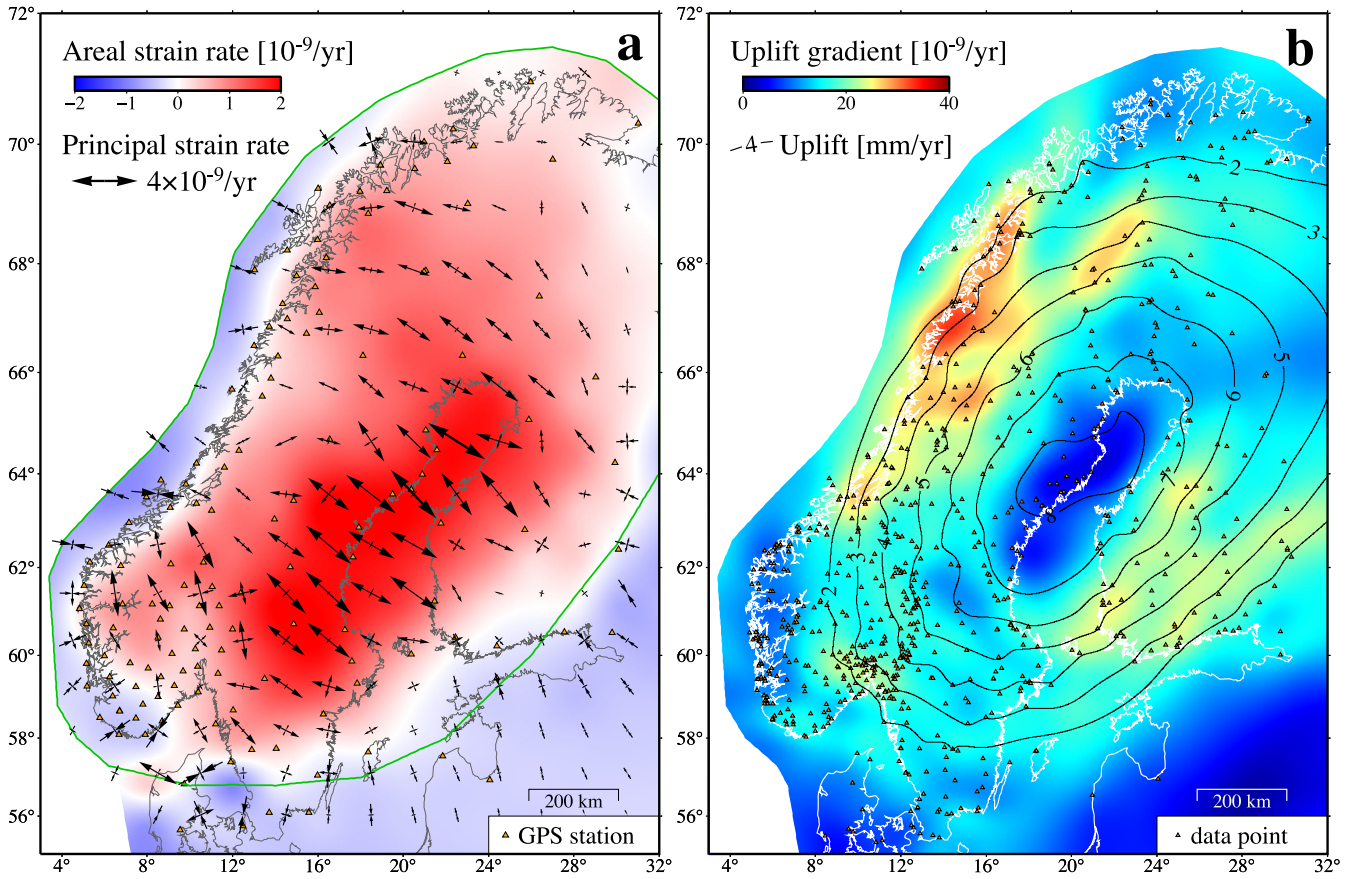

Figure 2. Surface deformation. (a) Horizontal areal strain rates (contour colours) and principal strain rates (arrows), based on GPS velocities from Kierulf *et al.* (2014). Positive values of areal strain rates indicate expansion and negative values indicate contraction in the horizontal plane. The green line shows the region used for the estimate of the total geodetic moment rate. (b) Uplift gradient based on GPS, levelling and tide-gauge data (Vestøl 2006). The gradient field has been smoothed with a spatial low pass filter before contouring.

areal strain occurs with equal shear strain on 45° dip-slip faults oriented at 90° to the principal horizontal strain directions, and that the remaining shear strain (the $\sqrt{\frac{1}{4}(\dot{\epsilon}_{xx} - \dot{\epsilon}_{yy})^2 + \dot{\epsilon}_{xy}{}^2}$ component of the formula) occurs on vertical strike-slip faults oriented at 45° to the principal strain directions. Any other dip angle requires a greater moment release, thus the moment rate formula yields a minimum estimate (Holt *et al.* 1995). Furthermore, the estimated moment rate only accounts for strain in the horizontal plane, thus the actual geodetic moment rate is probably higher. For the region encircled by the green line in Fig. 2(a), we estimate a total moment rate of 3.5×10^{18} Nm yr^{-1}, which we will later compare to estimates of the seismic moment rate from earthquakes.

An inspection of the velocity field in Fig. 1(a) indicates that the vertical strain rate may be several times larger than the horizontal strain rate. We are not able to calculate the strain rate in the vertical direction because we have no constraints on how the velocities change with depth. A measure of the vertical strain can, however, be obtained by considering the horizontal gradient of the uplift, defined as $\frac{\partial v_z}{\partial x} + \frac{\partial v_z}{\partial y}$, where v is velocity, z is vertical, x is longitude and y is latitude, as before. We calculate the uplift gradient from the data of Vestøl (2006), which includes levelling and tide-gauge measurements in addition to the vertical GPS velocities. The estimated uplift gradient field (Fig. 2b) shows a clear maximum in Nordland, where the two shallow earthquake swarms and Fennoscandia's largest earthquake were recorded, and where present-day activity of small events is high (see Fig. 1b).

4 DEFORMATION AT SEISMOGENIC DEPTHS

We use the compilation of focal mechanisms from the Norwegian continental margin and mainland Fennoscandia to examine the style of seismic strain release. To avoid introducing artefacts due to poorly constrained focal mechanisms, we only include mechanisms with quality A/B (for the Norwegian mechanisms which have a quality rating) and magnitudes of at least 2, which leaves 126 of 224 mechanisms within the region shown in Fig. 3(a). The focal mechanisms are first transformed to moment tensors (e.g. Lay & Wallace 1995), assuming that all magnitudes are equal to moment magnitudes (M_W), related to moments by the empirical relationship $\log M_0 = \frac{3}{2}M_W + 9.0$ (Hanks & Kanamori 1979). For clusters of events we calculate one average moment tensor, weighted by the earthquake moments. We then rotate each moment tensor into the principal-axis system to determine the maximum compressional and tensional deformation in the horizontal plane. The results are shown in Fig. 3(a). On the continental margin, the focal mechanisms show consistent WNW–ESE compression. In mainland Fennoscandia, the mechanisms show more variation between tension, compression and strike-slip and the directions are also seen to vary. The axes of compression often trend approximately NW–SE, consistent with the direction on the continental margin, but deviations from this pattern are seen in Nordland and near the Swedish coast to the Gulf of Bothnia. The variation in mainland Fennoscandia is partly due to the fact that the earthquakes are often small and therefore

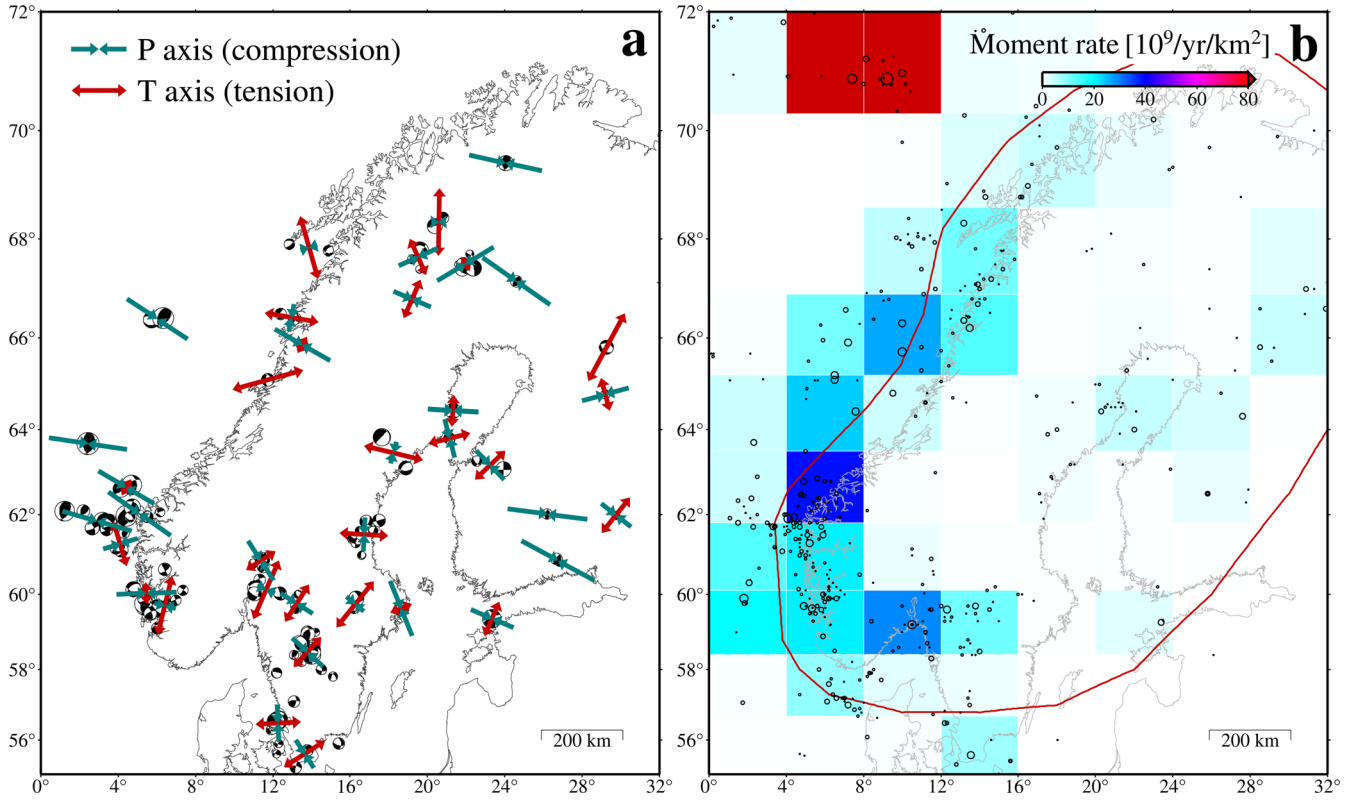

Figure 3. Deformation at seismogenic depth. (a) Focal mechanisms with horizontal P (compression) and T (tension) axes. Note that each pair of P and T axes only reflects the relative magnitudes of the two axes, not their absolute magnitudes relative to other events or event clusters. (b) Moment rates from summation of earthquake moments during 1900–2011 from the FENCAT catalogue. The red line shows the region used for the estimate of the total seismic moment rate.

more prone to reflect local conditions related to weakness zones or stress perturbations. However, a larger variation and a tendency towards tensional deformation in mainland Fennoscandia, compared to the continental margin, seem to be robust features, also when we consider only the larger events.

In order to quantify the seismic strain release, we calculate seismic moment rates from historical earthquakes. Here, we use all earthquakes from FENCAT during 1900–2011 to take advantage of the improvement of the completeness of the earthquakes records obtained after the onset of instrumental earthquake recordings around the beginning of the 20th century. We assume that the earthquake magnitudes are moment magnitudes, sum the moments on a grid and normalize the results to the area of each grid cell. The estimated moment rates in Fig. 3(b) show a coherent zone of high rates along the continental margin and along the western coast of Norway, and considerably lower rates further inland. As a side note, we see very high moment rates in the oceanic Lofoten Basin, where a seismic sequence occurred in 1959. The total seismic moment rate within the area encircled by the red line in Fig. 3(b) is 0.8×10^{16} Nm yr^{-1}, which is more than two orders of magnitude smaller than the geodetic moment rate within the same area.

Although the moment rates from the summation of historical earthquake moments show a relatively coherent pattern, the time period of a little more than hundred years only covers a fraction of the estimated return time of the largest events in Fennoscandia (Bungum *et al.* 2005), causing uncertainty on the derived moment rate estimate from historical earthquakes. We obtain a second, independent, estimate by calculating the expected seismic moment rate within the area encircled by the red line in Fig. 3(b), using the magnitude–frequency distribution of earthquakes during 1980–2011 and the formula of Molnar (1979):

$$\dot{M}_0^S = \frac{\alpha}{1-\beta} M_{0,\max}{}^{1-\beta}, \quad \alpha = 10^{(a+6b)}, \quad \beta = \frac{2}{3}b. \tag{3}$$

Here $M_{0,\max}$ is the moment of the expected largest possible earthquake in the region, and a and b are constants related to the magnitude–frequency relationship $\log_{10}N = a - bM$, where N is the annual number of events with magnitudes greater or equal to M. We obtain a maximum likelihood estimate of b (Utsu 1966; Marzocchi & Sandri 2003), and we estimate the a value from the intersection of the maximum likelihood line with the y-axis. The estimate of the expected moment rate is very dependent on the maximum moment, $M_{0,\max}$, which we do not know in detail. The largest historical earthquake in Fennoscandia had a magnitude of 5.8, as mentioned above. For the Norwegian continental margin, a maximum earthquake magnitude of 6–7 has been estimated (Bungum *et al.* 2005), and the maximum magnitude in mainland Fennoscandia is probably at the lower end of this range. If we assume that a maximum moment equivalent of an M_w=6.0 event is representative for the region within the red line in Fig. 3(b), we get a total moment rate of 1.3×10^{16} Nm yr^{-1}, which is in reasonable agreement with the estimate of 0.8×10^{16} Nm yr^{-1} from summation of historical earthquakes, suggesting that the inferred seismic moment rate is stable. In any case, the seismic moment rate is at least two orders of magnitude smaller than the geodetic moment rate from the horizontal strain rates.

5 DISCUSSION

Our analysis of the deformation at the surface (from geodetic data) and at seismogenic depth (from earthquake data) shows that there are large differences in the moment rates and to some extent also the style of deformation. The seismic moment rate in mainland Fennoscandia is at least two orders of magnitude smaller than the geodetic moment rate estimated from surface strain rates. A comparison of the style and direction of the strain rates shows slightly better agreement. In mainland Fennoscandia, where the surface deformation is dominated by a broad signal of extensional strain (see Fig. 2a), the focal mechanisms do show a tendency towards tensional deformation, but the pattern is more varied and the directions are often opposite to the NW–SE extension at the surface (see Fig. 3a). On the continental margin, there may be a better agreement, with NW–SE shortening in both the surface and seismic strain rate fields, but at the current stage, the comparison is much limited as we do not have surface observations offshore.

This raises the question why there is such discrepancy between the deformation at the surface and at seismogenic depth. While the GIA clearly dominates the surface strain rate field, its influence on the seismic deformation is not obvious. In order to explain this, we have to consider how GIA influences the deformation at the surface and at depth.

There is a depth dependency of the flexural stress and strain induced by GIA. The flexural stress decreases from the surface to zero at mid-lithospheric depth and then increase again with opposite sign towards the bottom of the lithosphere. Considering that most earthquakes in Fennoscandia occur in the upper 20 km of the crust, this depth dependency of the flexure could explain a moment difference of up to 40 per cent between the surface and seismogenic depth in a 100 km thick lithosphere, but this is much less than the observed difference. We do not consider it likely that the actual deformation at seismogenic depth is completely different from the surface strain rate, thus the deformation at seismogenic depth likely occurs mostly aseismically. But why is the strain induced by GIA not released in earthquakes?

The seismicity occurs in response to the state of stress, which in Fennoscandia is a result of the interaction of the regional stress field, flexural stress due to GIA as well as other stress generating mechanisms (e.g. Bungum *et al.* 2010). The regional, or tectonic, stress field seems to be controlled by plate boundary forces, which, in Fennoscandia, is primarily the ridge push from the Mid-Atlantic spreading ridge. This ridge push causes deviatoric NW–SE compression, which is consistent with the general trend of focal mechanisms, as also pointed out by, for example, Lindholm *et al.* (2000).

The stress induced by GIA depends on the ice history and mantle relaxation time, in addition to lithospheric thickness. During glaciation, the ice load causes downward flexure of the lithosphere, which results in contractional strain at the surface and compressive stress in the upper part of the down-bending lithosphere. After the onset of deglaciation, the upward flexure causes extensional strain at the surface and a change of the stress in the upper lithosphere towards less compressional or even tensional, depending on how much of the stress induced by the ice load had relaxed before the onset of deglaciation. Fig. 4(a) shows the case where no stress relaxation has occurred. In this case, the flexural stress in the upper part of the uplifting lithosphere will gradually become less compressive until it reaches zero as the uplift ends. Fig. 4(b) shows the other end-member case, where the lithosphere has reached equilibrium with the ice load before the onset of deglaciation. In this case, the flexural stress in the upper part of the uplifting lithosphere will be

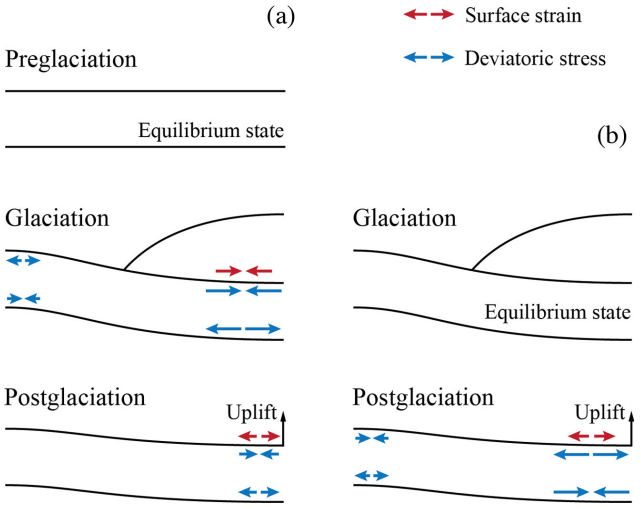

Figure 4. Two end-member cases for describing flexural stress induced by glacial isostatic adjustment. (a) No relaxation of the stress due to the ice load has occurred before the onset of deglaciation. (b) The stress due to the ice load has completely equilibrated before the onset of deglaciation. The figure is adapted from Fejerskov & Lindholm (2000, fig. 5).

tensional from the onset of deglaciation. Numerical evaluation of stress generating mechanisms in Fennoscandia shows that such tensional stress may reach a magnitude comparable to the stress from ridge push, if the lithosphere was in equilibrium with the ice load (Stein *et al.* 1989; Fejerskov & Lindholm 2000). Considering common relaxation times, the Fennoscandian glaciation history with frequent loading and unloading during the last 110 000 yr makes it unlikely that the lithosphere had reached equilibrium before the onset of deglaciation (Holger Steffen, private communication, 2014), but some stress relaxation probably had occurred.

The considerable tensional component of many focal mechanisms in mainland Fennoscandia suggests that the present-day stress is in fact influenced by tensional flexural stress due to GIA. This was previously suggested by Arvidsson & Kulhanek (1994) for Fennoscandia and similarly by Stein *et al.* (1979) for the Laurentide region. On the Norwegian continental margin, the variation between compressional and strike-slip focal mechanisms indicates that the minimum compressive horizontal stress and the vertical stress at seismogenic depth are of similar magnitudes. If the flexural stress in mainland Fennoscandia is characterized by NW–SE tension, similar to the pattern of the surface strain rates, then the interaction of the regional stress and the GIA stress will cause the NW–SE stress to become less compressional, such that the three principal stresses become more similar in magnitude (Fig. 5). The GIA induced accumulation of strain in the NW–SE direction, therefore, leads to decreased differential stress and thus a decrease in seismicity. On the continental margin, the flexural stress will be small in magnitude, but it will interfere constructively with the stress from ridge push to slightly increase the NW–SE compressional stress.

Our analysis follows along the lines of the study by Muir-Wood (2000), who ascribed the present-day seismicity in Fennoscandia to the interaction of ridge push and GIA stress. While we note that the occurrence of seismicity also reflects other conditions than the stress field, such as crustal heterogeneity and pre-existing weakness zones, we agree that the very low level of seismicity and more mixed style of seismic deformation in mainland Fennoscandia may be explained by the destructive interference of the regional stress with the GIA stress. Interestingly, the

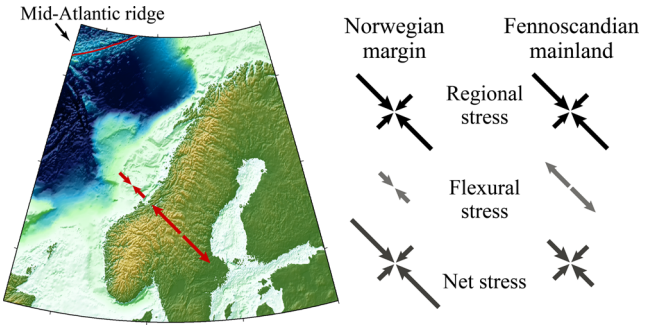

Figure 5. Schematic illustration of the hypothesized stress at seismogenic depth, illustrating the interaction of the regional stress due to the mid-Atlantic ridge push and the flexural stress due to glacial isostatic adjustment. The red arrows indicate surface strain.

relatively high seismicity in southwestern Norway occurs within the region of areal expansion, but the extension here deviates from the general NW–SE trend, which could lead to a less destructive interference.

The occurrence of seismicity in Nordland, where the uplift gradient is also high, may indicate that GIA plays a role in generating seismicity in this region. However, it has also been suggested that the high uplift gradient in the region is partly due to flexure induced by recent sediment redistribution (Olesen *et al.* 2013b). Furthermore, the Nordland region is characterized by deep fjords and steep mountains, making it likely that gravitational stresses due to the high topography contrasts increase seismicity levels.

6 CONCLUSIONS

We investigate how GIA influences the state of stress and deformation in Fennoscandia, through analysis of surface strain rates and seismicity.

(1) The surface strain rate field, derived from horizontal GPS data, shows a signal of expansion that covers most of mainland Fennoscandia with extensional strain rates of up to 4×10^{-9} yr^{-1} in the NW–SE direction.

(2) The uplift gradient, derived from a combination of GPS, levelling and tide-gauge measurements, shows the highest deformation rates in Nordland, Norway, where seismicity is also high.

(3) The seismic deformation field, derived from a new compilation of Fennoscandian focal mechanisms, shows consistent NW–SE shortening on the Norwegian continental margin and a more mixed deformation pattern in mainland Fennoscandia.

(4) The seismic moment rate, derived from historical earthquakes as well as the moment–frequency relationship of recent earthquakes, is at least two orders of magnitude smaller than the geodetic moment rate derived from the GPS strain rates.

Our analyses indicate that the GIA influences the present-day state of stress in Fennoscandia by diminishing the NW–SE compressional stress due to the ridge push from the Mid-Atlantic ridge. This leads to low differential stress and thus low seismicity rates with highly variable focal mechanisms in mainland Fennoscandia. Other sources of stress such as high topography and flexuring due to sediment redistribution may also influence the state of stress in Fennoscandia, particularly in southwestern Norway and Nordland. Future numerical modelling may help distinguishing between the potential sources of seismicity in Fennoscandia.

ACKNOWLEDGEMENTS

We wish to thank Hilmar Bungum for fruitful discussions and comments on the paper. Lars Ottemöller from University of Bergen did a careful evaluation the new focal mechanisms from the Norwegian National Seismic Network, and Marja Uski and Björn Lund kindly assisted with the focal mechanisms from Finland and Sweden. Constructive reviews from two anonymous reviewers helped improve the manuscript. The FENCAT earthquake catalogue of the University of Helsinki, Finland, is available at http://www.helsinki.fi/geo/seismo/ (last accessed 28 May 2015). The figures were prepared with GMT (Wessel *et al.* 2013). This work was supported by the Geological Survey of Norway, the Norwegian Research Council, Norwegian Petroleum Directorate, Det norske oljeselskap, DONG E&P Norge, E.ON E&P Norge, Lundin Norway, Maersk Oil Norway, Norske Shell, Norwegian Energy Company (Noreco), Repsol Exploration Norge, DEA Norge, Statoil and VNG Norge.

REFERENCES

Arvidsson, R., 1996. Fennoscandian earthquakes: whole crustal rupturing related to postglacial rebound, *Science*, **274**(5288), 744–746.

Arvidsson, R. & Kulhanek, O., 1994. Seismodynamics of Sweden deduced from earthquake focal mechanisms, *Geophys. J. Int.*, **116**(2), 377–392.

Atakan, K., Lindholm, C.D. & Havskov, J., 1994. Earthquake swarm in Steigen, northern Norway: an unusual example of intraplate seismicity, *Terra Nova*, **6**(2), 180–194.

Beavan, J. & Haines, J., 2001. Contemporary horizontal velocity and strain rate fields of the Pacific-Australian plate boundary zone through New Zealand, *J. geophys. Res.*, **106**(B1), 741–770.

Bird, P. & Kagan, Y.Y., 2004. Plate-tectonic analysis of shallow seismicity: apparent boundary width, beta, corner magnitude, coupled lithosphere thickness, and coupling in seven tectonic settings, *Bull. seism. Soc. Am.*, **94**(6), 2380–2399.

Bøe, R., Fossen, H. & Smelror, M., 2010. Mesozoic sediments and structures onshore Norway and in the coastal zone, *NGU Bulletin*, **450**, 15–32.

Bungum, H. & Olesen, O., 2005. The 31st of August 1819 Lurøy earthquake revisited, *Norw. J. Geol.*, **85**, 245–252.

Bungum, H., Vaage, S. & Husebye, E.S., 1982. The Meløy earthquake sequence, northern Norway: Source parameters and their scaling relations, *Bull. seism. Soc. Am.*, **72**(1), 197–206.

Bungum, H., Lindholm, C. & Faleide, J.I., 2005. Postglacial seismicity offshore mid-Norway with emphasis on spatio-temporal-magnitudal variations, *Mar. Pet. Geol.*, **22**(1–2), 137–148.

Bungum, H., Olesen, O., Pascal, C., Gibbons, S., Lindholm, C. & Vestøl, O., 2010. To what extent is the present seismicity of Norway driven by post-glacial rebound?, *J. Geol. Soc.*, **167**, 373–384.

Byrkjeland, U., Bungum, H. & Eldholm, O., 2000. Seismotectonics of the Norwegian continental margin, *J. geophys. Res.*, **105**(B3), 6221–6236.

Dehls, J.F., Olesen, O., Olsen, L. & Blikra, L.H., 2000. Neotectonic faulting in northern Norway; the Stuoragurra and Nordmannvikdalen postglacial faults, *Quat. Sci. Rev.*, **19**(14–15), 1447–1460.

Ekström, G., Nettles, M. & Dziewoóski, A.M., 2012. The global CMT project 2004–2010: Centroid-moment tensors for 13,017 earthquakes, *Phys. Earth planet. Inter.*, **200–201**, 1–9.

Fejerskov, M. & Lindholm, C., 2000. Crustal stress in and around Norway: an evaluation of stress-generating mechanisms, *Geol. Soc. Lond.*, **167**, 451–467.

Hanks, T.C. & Kanamori, H., 1979. A moment magnitude scale, *J. geophys. Res.*, **84**(B5), 2348–2350.

Hasegawa, H.S. & Basham, P.W., 1989. Spatial correlation between seismicity and postglacial rebound in eastern Canada, in *Earthquakes at North-Atlantic Passive Margins: Neotectonics and Postglacial Rebound*, pp. 483–500, eds Gregersen, S. & Basham, P.W., NATO ASI Series.

Henderson, J., 1991. An estimate of the stress tensor in Sweden using earthquake focal mechanisms, *Tectonophysics*, **192**(3–4), 231–244.

Hicks, E.C. & Ottemöller, L., 2001. The ML 4.5 Stord/Bømlo, southwestern Norway, earthquake of 12 August 2000, *Norsk Geologisk Tidsskrift*, **81**, 293–304.
Hicks, E.C., Bungum, H. & Lindholm, C.D., 2000a. Stress inversion of earthquake focal mechanism solutions from onshore and offshore Norway, *Norsk Geologisk Tidsskrift*, **80**, 235–250.
Hicks, E.C., Bungum, H. & Lindholm, C.D., 2000b. Seismic activity, inferred crustal stresses and seismotectonics in the Rana region, Northern Norway, *Quat. Sci. Rev.*, **19**(14–15), 1423–1436.
Holt, W.E., Li, M. & Haines, A.J., 1995. Earthquake strain rates and instantaneous relative motions within central and eastern Asia, *Geophys. J. Int.*, **122**, 569–593.
Holt, W.E., Chamot-Rooke, N., Le Pichon, X., Haines, A.J., Shen-Tu, B. & Ren, J., 2000. Velocity field in Asia inferred from Quaternary fault slip rates and Global Positioning System observations, *J. geophys. Res.*, **105**(B8), 19 185–19 209.
Juhlin, C. & Lund, B., 2011. Reflection seismic studies over the end-glacial Burträsk fault, Skellefteå, Sweden, *Solid Earth*, **2**, 9–16.
Kierulf, H.P., Ouassou, M., Simpson, M. J.R. & Vestøl, O., 2013. A continuous velocity field for Norway, *J. Geod.*, **87**(4), 337–349.
Kierulf, H.P., Steffen, H., Simpson, M.J.R., Lidberg, M., Wu, P. & Wang, H., 2014. A GPS velocity field for Fennoscandia and a consistent comparison to glacial isostatic adjustment models, *J. geophys. Res.*, **119**(8), 6613–6629.
Kreemer, C., Blewitt, G. & Klein, E.C., 2014. A geodetic plate motion and Global Strain Rate Model, *Geochem. Geophys. Geosyst.*, **15**(10), 3849–3889.
Lagerbäck, R., 1992. Dating of Late Quaternary faulting in northern Sweden, *J. geol. Soc. Lond.*, **149**, 285–291.
Lay, T. & Wallace, T.C., 1995. *Modern Global Seismology*, Academic Press.
Lidberg, M., Johansson, J.M., Scherneck, H.-G. & Milne, G.A., 2010. Recent results based on continuous GPS observations of the GIA process in Fennoscandia from BIFROST, *J. Geodyn.*, **50**(1), 8–18.
Lindblom, E., Lund, B., Tryggvason, A., Uski, M., Bödvarsson, R., Juhlin, C. & Roberts, R., 2015. Microearthquakes illuminate the deep structure of the endglacial Pärvie fault, northern Sweden, *Geophys. J. Int.*, **201**, 1704–1716.
Lindholm, C.D., Bungum, H., Hicks, E. & Villagran, M., 2000. Crustal stress and tectonics in Norwegian regions determined from earthquake focal mechanisms, *Geol. Soc. London Spec. Publ.*, **167**, 429–439.
Lindholm, C., Roth, M., Bungum, H. & Faleide, J.I., 2005. Probabilistic and deterministic seismic hazard results and influence of the sedimentary Møre Basin, NE Atlantic, *Mar. Pet. Geol.*, **22**(1–2), 149–160.
Lund, B., Schmidt, P. & Hieronymus, C., 2009. *Stress evolution and fault stability during the Weichselian glacial cycle, Tech. Rep. TR-09-15*, Swedish Nuclear Fuel and Waste Management Co, Stockholm, Sweden.
Mäntyniemi, P., Husebye, E.S., Kebeasy, T. R.M., Nikonov, A.A., Nikulin, V. & Pacesa, A., 2004. State-of-the-art of historical earthquake research in Fennoscandia and the Baltic Republics, *Ann. Geophys.*, **47**(2/3), 611–619.
Marzocchi, W. & Sandri, L., 2003. A review and new insights on the estimation of the b-value and its uncertainty, *Ann. Geophys.*, **46**(6), 1271–1282.
Mazzotti, S., James, T.S., Henton, J. & Adams, J., 2005. GPS crustal strain, postglacial rebound, and seismic hazard in eastern North America: The Saint Lawrence valley example, *J. geophys. Res.*, **110**(B11), 1–16.
Molnar, P., 1979. Earthquake recurrence intervals and plate tectonics, *Bull. seism. Soc. Am.*, **69**(1), 115–133.
Muir Wood, R., 1989a. The Scandinavian earthquakes of 22 December 1759 and 31 August 1819, *Disasters*, **12**(3), 223–236.
Muir Wood, R., 1989b. Extraordinary deglaciation reverse faulting in northern Fennoscandia, in *Earthquakes at North-Atlantic Passive Margins: Neotectonics and Postglacial Rebound*, pp. 141–173, eds Gregersen, S. & Basham, P.W., NATO ASI Series.
Muir-Wood, R., 2000. Deglaciation Seismotectonics: a principal influence on intraplate seismogenesis at high latitudes, *Quat. Sci. Rev.*, **19**(14–15), 1399–1411.
Nocquet, J.-M., Calais, E. & Parsons, B., 2005. Geodetic constraints on glacial isostatic adjustment in Europe, *Geophys. Res. Lett.*, **32**(6), 1–5.
Olesen, O., Bungum, H., Dehls, J., Lindholm, C., Pascal, C. & Roberts, D., 2013a. Neotectonics, seismicity and contemporary stress field in Norway – mechanisms and implications, *NGU Spec. Publ.*, **13**, 145–174.
Olesen, O., Kierulf, H.P., Brönner, M., Dalsegg, E., Fredin, O. & Solbakk, T., 2013b. Deep weathering, neotectonics and strandflat formation in Nordland, northern Norway, *Norw. J. Geol.*, **93**, 189–213.
Ottemöller, L., Nielsen, H.H., Atakan, K., Braunmiller, J. & Havskov, J., 2005. The 7 May 2001 induced seismic event in the Ekofisk oil field, North Sea, *J. geophys. Res.*, **110**(B10), 1–15.
Riis, F. & Fjeldskaar, W., 1992. On the magnitude of the late Tertiary and Quaternary erosion and its significance for the uplift of Scandinavia and the Barents Sea, in *Structural and Tectonic Modelling and its Applications to Petroleum Geology*, Vol. 1 of NPF Special Publication, pp. 163–185, eds Larsen, R.M., Brekke, H., Larsen, B.T. & Talleraas, E., Elsevier.
Slunga, R., 1979. Source mechanisms of a Baltic earthquake inferred from surface-wave recordings, *Bull. seism. Soc. Am.*, **69**(6), 1931–1964.
Slunga, R. & Ahjos, T., 1986. Fault mechanisms of Finnish earthquakes, crustal stresses and faults, *Geophysica*, **22**(1–2), 1–13.
Smedberg, I., Uski, M., Tiira, T., Komminaho, K. & Korja, A., 2012. Intraplate earthquake swarm in Kouvola, south-eastern Finland, in *EGU General Assembly 2012*, Vienna, Austria.
Sørensen, M.B., Ottemöller, L., Havskov, J., Atakan, K., Hellevang, B. & Pedersen, R.B., 2007. Tectonic processes in the Jan Mayen Fracture Zone based on earthquake occurrence and bathymetry, *Bull. seism. Soc. Am.*, **97**(3), 772–779.
Steffen, H. & Wu, P., 2011. Glacial isostatic adjustment in Fennoscandia – A review of data and modeling, *J. Geodyn.*, **52**(3–4), 169–204.
Stein, S., Sleep, N.H., Geller, R.J., Wang, S.-C. & Kroeger, G.C., 1979. Earthquakes along the passive margin of eastern Canada, *Geophys. Res. Lett.*, **6**(7), 537–540.
Stein, S., Cloething, S., Sleep, N.H. & Wortel, R., 1989. Passive margin earthquakes, stresses and rheology, in *Earthquakes at North-Atlantic Passive Margins: Neotectonics and Postglacial Rebound*, pp. 231–259, eds Gregersen, S. & Basham, P.W., NATO ASI Series.
Uski, M., Hyvönen, T., Korja, A. & Airo, M.-L., 2003. Focal mechanisms of three earthquakes in Finland and their relation to surface faults, *Tectonophysics*, **363**(1–2), 141–157.
Uski, M., Tiira, T., Korja, A. & Elo, S., 2006. The 2003 earthquake swarm in Anjalankoski, south-eastern Finland, *Tectonophysics*, **422**, 55–69.
Utsu, T., 1966. A statistical significance test of the difference in the b-value between two earthquake groups, *J. Phys. Earth*, **14**(2), 37–40.
Vestøl, O., 2006. Determination of postglacial land uplift in Fennoscandia from leveling, tide-gauges and continuous GPS stations using least squares collocation, *J. Geod.*, **80**(5), 248–258.
Wessel, P., Smith, W. H.F., Scharroo, R., Luis, J. & Wobbe, F., 2013. Generic Mapping Tools: improved version released, *EOS, Trans. Am. geophys. Un.*, **94**(45), 409–410.
Wu, P. & Johnston, P., 2000. Can deglaciation trigger earthquakes in N. America?, *Geophys. Res. Lett.*, **27**(9), 1323–1326.

SUPPORTING INFORMATION

Additional Supporting Information may be found in the online version of this paper:

Table S1. Fennoscandian earthquake focal mechanisms.
Figure S1. Location and depth distribution of focal mechanisms in Table S1. (http://gji.oxfordjournals.org/lookup/suppl/doi:10.1093/gji/ggv207/-/DC1).

Please note: Oxford University Press is not responsible for the content or functionality of any supporting materials supplied by the authors. Any queries (other than missing material) should be directed to the corresponding author for the paper.